Journal of Sustainable Development of Energy, Water and Environment Systems

http://www.sdewes.org/jsdewes

Year 2026, Volume 14, Issue 4, 1140732

*Original Research Article*

# Analytical Modelling and Design of a Submersible Threshold Hydraulic Micro-Dam to Evaluate Rural Hydroelectric Production on Non-Diverted Low-Head Rivers

***Parfait Koua-Mbani*** [*1,2], ***Mathieu Liassa Nkoy***[3], ***Franck Moukanda Mbango***[1,2,4]

[1]École Nationale Supérieure Polytechnique (ENSP), Université Marien Ngouabi (UMNG), BP 69, Brazzaville, République du Congo
e-mail: parfait.koua-mbani@umng.cg

[2]Laboratoire de Génie Électrique et Électronique, Université Marien Ngouabi (U.M.NG), BP 69, Brazzaville, République du Congo

[3]Laboratory of Electrotechnical and Electrical Machines, Polytechnic Faculty, University of Kinshasa (UNIKIN), Kinshasa, Democratic Republic of Congo
e-mail: mathieu.liassa@unikin.ac.cd

[4]Faculty of Science and Techniques (FST), University of Marien Ngouabi (U.M.NG), BP 69, Brazzaville, Republic of the Congo
e--mail: franck.moukandambango@umng.cg

Cite as: Koua-Mbani, P., Liassa Nkoy, M., Moukanda Mbango, F., Analytical Modelling and Design of a Submersible Threshold Hydraulic Micro-Dam to Evaluate Rural Hydroelectric Production on Non-Diverted Low-Head Rivers, J.sustain. dev. energy water environ. syst., 14(4), 1140732, 2026, DOI: https://doi.org/10.13044/j.sdewes.d14.0732



## ABSTRACT

This study presents the analytical modelling, design, and hydraulic validation of a submersible threshold hydraulic micro-dam for rural hydroelectric production on non-diverted low-head rivers. Installed directly in the river, this micro-dam offers a technically and economically viable solution to meet the growing electricity demand in rural sub-Saharan communities, particularly in the Republic of Congo, while promoting renewable technologies and sustainable development. This work's contribution is the development and validation of a simplified analytical model derived from the 1D Saint-Venant equations, systematically compared with two-dimensional numerical simulations in COMSOL Multiphysics, applied to a case study of the Douni River in the Republic of Congo. The analytical model enables the estimation of flow speed distributions, pressures, and hydraulic power along the micro-dam channels. Results indicate average flow speeds of 4.46-9.82 m/s per channel, far exceeding the measured river velocity of 0.297 m/s. Hydraulic power outputs of 7.13 kW to 28.96 kW per channel (14.26-57.92 kW for a two-channel system) for water depths ranging from 0.22 m to 0.10 m under supercritical flow conditions. The average relative deviation between the analytical and the numerical simulation results remains below 5%, confirming the validity of the proposed simplified method for preliminary design. These values correspond to a maximum slope of 21.8° (40% per channel) and a minimum drop of 1 m. The submersible threshold hydraulic micro-dam demonstrates potential as an integrated hydraulic-hydroelectric solution for small rivers in rural villages, where conventional flow diversion is limited by the absence of natural slopes and high banks. This study is limited to two-dimensional simulations and uniform steady-state flow assumptions and provides a reliable basis for designing low-cost, sustainable micro-hydroelectric systems for electrification in remote areas.

## KEYWORDS

*Saint-Venant equations; Submersible micro-dam; micro-hydropower; turbulent flow; rural electrification*

[*] Corresponding author

## INTRODUCTION

Rural electrification is a central issue in Africa, where nearly 600 million people lack consistent access to electricity, and the average rural electrification rate in sub-Saharan Africa is only 34%. In the Republic of the Congo, the situation is more critical despite an estimated hydroelectric potential of 27,000 MW; only 1% is currently exploited in 2025, and electrification rates were 49% in urban areas and only 12% in rural areas. This significantly hinders the development of the economic and social environment in isolated regions, as grid extension to remote areas remains technically and economically challenging [1], [2].The resolution of these problems also requires an off-grid electrification approach that exploits local resources. Decentralized systems based on renewable energies offer a credible alternative. Among them, micro-hydroelectricity occupies a privileged position due to its continuous production and low carbon footprint. Hydropower is both one of the most widely used renewable energy sources and the largest single contributor to global electricity generation, supplying approximately 14.3% of global power generation in 2024 and supporting power system flexibility in more than 150 countries [3], [4]. The global hydropower fleet expanded by approximately 24.6 GW in 2024, including both conventional and pumped-storage capacity, underscoring its enduring role in the energy landscape.

Hydroelectric microsystems offer a sustainable and reliable means of directly harnessing hydraulic resources near villages, particularly rivers with very low or no head. Among the technologies, the submersible threshold hydraulic micro-dam (STHMD) offers the advantage of minimizing environmental impact while ensuring continuous energy production adapted to local needs [5], [6]. They represent an innovative solution for energy recovery in very low-fall rivers ($h<0.2$ m), as the geomorphological configuration of the watercourses makes it challenging to construct traditional diversions or leakage channels due to high banks, dense vegetation, and strong seasonal fluctuations in water level [7]. A submersible sill is a concrete structure at the riverbed that creates a controlled body of water without interrupting flow. This type of dam avoids the environmental impacts associated with conventional dams, promoting ecological continuity. With two parallel flow channels, the studied network provides a controlled distribution of flow to turbines, thereby increasing hydraulic stability and reducing energy losses due to turbulence [8]. The first design studies of submersible thresholds have highlighted the complexity of the interactions among upstream load, partial flooding, and energy dissipation [9], [10]. Experimental and numerical approaches have made it possible to identify the transient flow regimes between free and submerged threshold, notably via the Villemonte submerged-weir discharge equation 1947 [11], [12], and recent studies based on computational fluid dynamics (CFD) allow us to revisit this approach by explicitly resolving the transition between free and submerged flow regimes [13], [14]. Work on modelling gently sloping rectangular channels has evolved toward integrating the k-ε turbulence-coupled averaged Navier-Stokes equations to estimate the speed distribution and distributed head loss [15]. These validated models in software such as COMSOL and ANSYS Fluent enable analysis of the stability of the water profile as a function of slope and roughness [16]. Despite the progress, the study noted that the configuration examined is underrepresented in the literature. Several authors have explored single-channel configurations with forced lines, sometimes very long, on sites whose geomorphology favors overflows, falls, or natural elevations ranging from 3 to 5m [17], [18]. In addition, little research addresses the short double-channel configuration with a submersible threshold placed directly in the river, oriented downstream, creating an artificial fall greater than 0.50 m as an integrated system, which constitutes the main contribution of this study. Flow control in each channel is typically achieved using flat steel gates [19]. The complete modelling of this STHMD with two identical channels in parallel presents the challenges of precise calculations of the flow distribution influenced by the geometry of the threshold and the pressure losses, the prediction of the non-uniform flow regime and dynamic submersion conditions, and the evaluation of the hydraulic power

available for each channel before mechanical conversion. These aspects require a Multiphysics approach that couples the flow and energy equations through experimentally validated CFD simulations. Several commercial and research tools are commonly used for open-channel flow analysis and hydraulic design, including numerical modelling software such as HEC-RAS, MIKE 21, ANSYS Fluent, and COMSOL Multiphysics. These tools provide detailed simulations of flow behaviour, often using multidimensional numerical methods. However, their application generally requires advanced computational resources and specialized expertise, which may limit their use in rural or resource-constrained environments. In this context, the present study aims to model and design a STHMD under real operating conditions and to develop a simplified analytical hydraulic model for predicting flow behaviour in such configurations. The originality of this work lies in the design of a STHMD configuration placed directly in the river, validated through a two-dimensional numerical simulation in COMSOL Multiphysics, ensuring its reliability for engineering applications. By systematically comparing analytical predictions with numerical results, this work provides a reliable framework for assessing flow distribution, speed, and hydraulic power in small rivers, highlighting the practical applicability of the analytical model for the preliminary design and optimization of low-cost, sustainable micro-hydropower solutions for rural hydroelectric projects.



## MATERIALS AND METHODS

This section presents the methodology adopted in this study, including the description of the study site, the hydrological data used, and the modelling approaches applied. It outlines the main assumptions, analytical formulations, and numerical tools employed to investigate the hydraulic behaviour and hydraulic energy potential of the proposed micro-dam system.

### Presentation of the site and hydrological data

The studied submersible threshold hydraulic micro-dam is intended for a river, the Douni (Figure 2), non-navigable with very low hydraulic head (<0.2m), typical of rural areas in the northern part of the Republic of Congo, in the basin department, in the sub-prefecture of Makoua, at the village of Issongo (Figure 1).

Figure 2. River Douni-village Issongo, Cuvette, Republic of the Congo.

Figure 1. Study area, River Douni-village Issongo, Cuvette, Republic of the Congo. Google map.

The system's measurement and installation area on the Douni River is located between two bridges: an old bridge on which the measurements were carried out, and the new bridge. The map (Figure 3) of the Douni River catchment illustrates the origin, quantification, and dynamics of the water that will supply the mid-dam with a submersible threshold.

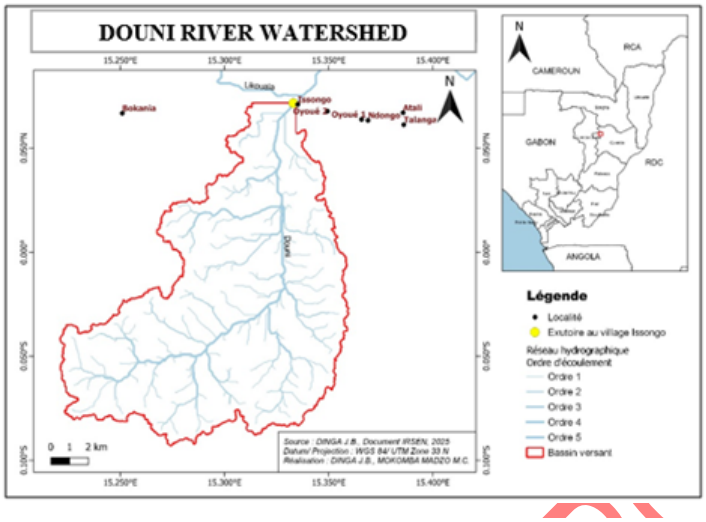


Figure 3. Map of the watershed of the river Douni. From Institut de Recherche en Sciences Exact et Naturelles (IRSEN) Congo.

This map indicates that basin characteristics determine reservoir size and hydraulic safety at the operating point (Issongo village) upstream of the Likouala Mossaka River. The measurement materials are specified in the methodology [20]. Different materials were used: the gauging method with a 25 kg Moulinet and a salmon (streamlined lead weight used in current metering) (Figure 6), consisting of a device with diameters of 125 and 100mm, a propeller from 0.125 to 0.500m, an electric pulse counter, and the electro-carrier cable wound on a winch (Figure 5). The movements are made along the vertical (depth) and horizontal axes. Distances via the winch throat for salmon gauging and a pole for pole gauging [21]. The salmon was attached to the winch mounted on a cantilever. The relationships for determining the average flow rate and the average velocities, various measurements are given as follows, (according the Figure 4) [22], [23] :

$$Q = lHV \tag{1}$$

which can also be written as given below:

$$Q = AV \tag{2}$$

where $l$ is the width of the section in meter $m$, $H$ is the average depth in $m$, $V$ is the average speed in $m.s^{-1}$, $A$ is the surface of the wet section in $m^2$, and $Q$ is the average flow rate in $m^3.s^{-1}$.

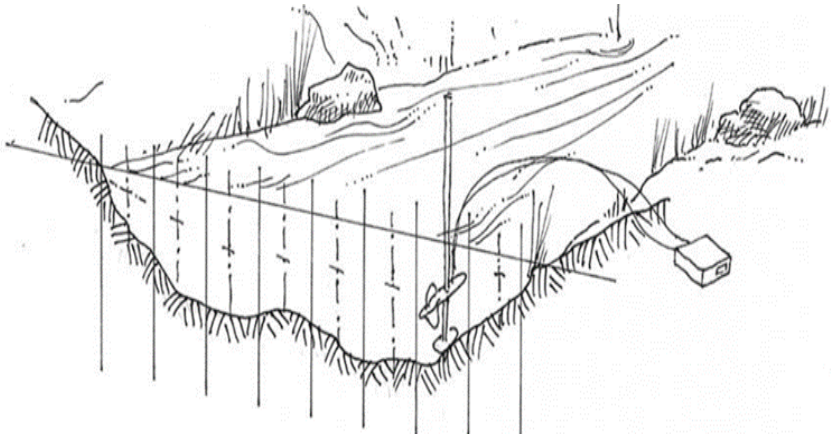

Figure 4. Representation of the speed area method, measuring flow rates and speeds [22]

Figure 6. Complete equipment (propeller, Reel, Salmon and tail)

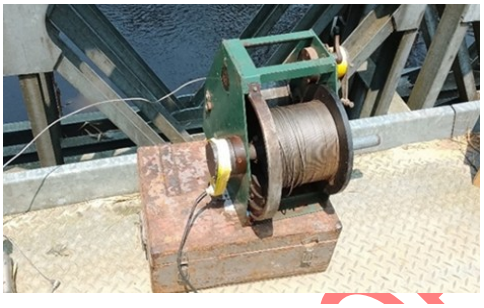

Figure 5. Manual winch used during measurements.

This enabled obtaining the following average values after several measurements and months of observation in Table 1.

**Table 1**. Average flow and speed of the Douni River, Issongo village

| Variables | Symbol | Unit | Values measured |
|---|---|---|---|
| Average flow rate | Q | $m^3/s$ | 1.178 |
| Average speed | $V_m$ | m/s | 0.297 |
| Wet section | $S_m$ | $m^2$ | 3.41 |
| Width river | $l$ | m | 7 |
| Max depth | $H_r$ | m | 0.9 |

The average speed obtained from various measurements was too low to drive turbines, and controlling flow relative to river depth should be complex during floods or periods of water scarcity. In addition, the site does not foresee any possibility of diverting the flow due to a lack of natural slopes. Therefore, the design of a micro-dam placed directly in the river enabled a small drop height to accelerate water flow.

## Geometric description of the hydraulic micro-dam

The system studied includes a submersible threshold hydraulic micro-dam (Figure 7 and Figure 8) mainly having: two rectangular smooth concrete channels, identical in water depth in the channel $h_i(x,t)$ with $i = 1,2$, a length L, a width b, and a bottom slope $S_0$; of a submersible threshold of width B, of height $h_s(x,t)$.

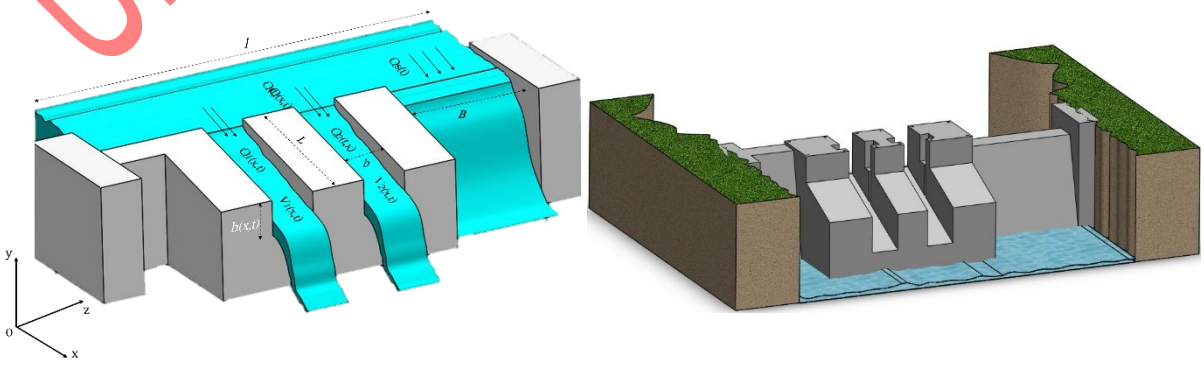

Figure 7. Representation of the flow profile in the channels and at the submersible threshold during flood periods.

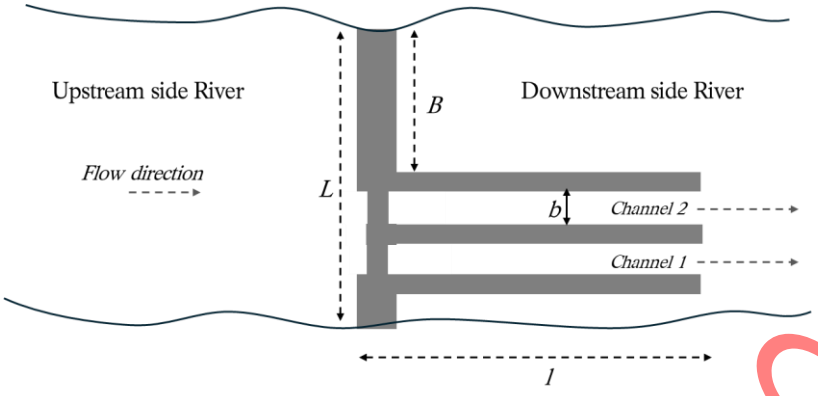


Figure 8. Conceptual representation of the studied network (STHMD)

**Design methodology of the micro-dam**

The design of the submersible threshold hydraulic micro-dam (STHMD) is based on a coupled hydraulic and energy approach that accounts for the specific constraints of non-diverted rivers. First, the site's hydrological characteristics are defined based on field measurements, including the average flow rate and the initial average flow speed. These parameters constitute the input data for the hydraulic modelling. The geometry of the micro-dam, as shown in Figure 7, including the threshold height, channel slope, and their cross-sectional dimensions, is then determined to create an artificial head while maintaining flow continuity. Particular attention is given to ensuring that the structure remains submerged under normal flow conditions, thus minimizing environmental impact. The STHMD was designed in SolidWorks for accurate dimensional representation.

The flow distribution in the two parallel channels is evaluated using an analytical model based on the Saint-Venant equations, which allows the estimation of flow speed, hydraulic power, Froude number, and the water surface profile along the channels. Based on these hydraulic parameters, the available hydraulic power for each channel is calculated, accounting for head losses and flow conditions. This step enables assessment of the system's energy production potential.

**Modelling of the hydraulic micro-dam with a submersible threshold**

Consider the network of the hydraulic micro-dam represented in Figure 7 and Figure 8 and the conceptual representation below (Figure 8), which consists of two channels and a submersible threshold. The prismatic rectangular channels are indexed by number $i(i = 1,2)$, for each channel it has been admitted: $h_i$ is the height of the water column (m), $Q_i$ is the flow rate of water in the channel ($m^3/s$), $L$ is the length of the channel (m), $b$ is the width of the channel (m), $B$ is the submersible sill width (m), and $l$ the river width (m).

**Formulation of fluid dynamics equations on the model STHMD**

The three-dimensional design of micro-hydraulic dams for electric power production requires rigorous modelling of flows governed by the Navier-Stokes equations [24], [25]. For a turbulent flow where all the transverse forces z, vertical y, and longitudinal x act on the fluid with a velocity having components $V_x$, $V_y$ and $V_z$ with $V_i(x, y, z, t)$, the water flow behavior at

the channel sections and the submersible sill can be modelled by the generalized form of the developed Navier-Stokes dynamic flow as follows :

$$\frac{\partial \rho}{\partial t} + \frac{\partial \rho V_x(x,y,z,t)}{\partial x} + \frac{\partial \rho V_y(x,y,z,t)}{\partial y} + \frac{\partial \rho V_z(x,y,z,t)}{\partial z} = 0 \quad (3)$$

$$\begin{cases} \rho\left\{\frac{\partial V_x(x,y,z,t)}{\partial t} + V_x\frac{\partial V_x(x,y,z,t)}{\partial x} + V_y\frac{\partial V_x(x,y,z,t)}{\partial y} + V_z\frac{\partial V_x(x,y,z,t)}{\partial z}\right\} = k_x \\ \rho\left\{\frac{\partial V_y(x,y,z,t)}{\partial t} + V_x\frac{\partial V_y(x,y,z,t)}{\partial x} + V_y\frac{\partial V_y(x,y,z,t)}{\partial y} + V_z\frac{\partial V_y(x,y,z,t)}{\partial z}\right\} = k_y \\ \rho\left\{\frac{\partial V_z(x,y,z,t)}{\partial t} + V_x\frac{\partial V_z(x,y,z,t)}{\partial x} + V_y\frac{\partial V_z(x,y,z,t)}{\partial y} + V_z\frac{\partial V_z(x,y,z,t)}{\partial z}\right\} = k_z \end{cases} \quad (4)$$

with,

$$\begin{cases} k_x = -\frac{\partial P(x,y,z,t)}{\partial x} + \rho g_x + \mu\nabla^2 V_x(x,y,z,t) \\ k_y = -\frac{\partial p(x,y,z,t)}{\partial y} + \rho g_y + \mu\nabla^2 V_y(x,y,z,t) \\ k_z = -\frac{\partial p(x,y,z,t)}{\partial z} + \rho g_z + \mu\nabla^2 V_z(x,y,z,t) \end{cases} \quad (5)$$

where: $\rho$ is the density of water (kg.m$^{-3}$), $g_f$ is the acceleration along the axis of the Cartesian mark (m$^2$.s$^{-1}$), $P(x,y,z,t)$ is the pressure (N.m$^{-2}$), and $\mu$ is the dynamic viscosity of water (kg.m$^{-1}$.s$^{-1}$).

The equation represents the conservation of water momentum as it flows over the projections of the Cartesian coordinate system. These equations enable linking the forces and dynamics of water by integrating the effects of gravity, pressure drops, and buoyancy forces to predict the actual behavior of water in our hydraulic structure. They are therefore essential for the design of hydraulic micro-dams with a movable threshold, where the distribution of velocities in the channels and pressures directly influence energy efficiency and hydraulic stability [26], [27]. The equation represents the conservation of mass, also called the continuity equation. It links velocity variations to channel geometry, thus allowing the determination of local speeds from wet sections and flow rates, which provide the basis for modelling flows in our channels and jets for the implementation of cross-flow turbines [28].

**Modelling of the channels of the studied network**

Modelling the flow channels of the studied network involves establishing the 1D Saint-Venant equations. For the studied network, different assumptions are considered for applying the Navier-Stokes equations to the hydraulic network shown in Figure 8. Flow projection in the channels is performed longitudinally. Since water is an incompressible Newtonian fluid, the viscosity remains constant regardless of the applied stress, and the volume remains constant per unit, with respect to the bottom slope italicized, the frictions are turbulent and modeled by the hydraulic slope $S_{f,i}$ ; lateral contributions are treated as inputs (rains, etc.) per unit of length with $q_{l,i}(x,t)$ lateral flow and $v_{l,i}(x,t)$ lateral speed. The transverse and vertical speeds are considered very low compared to the longitudinal speed along the channels, relative to the bottom slope $S_0$ . By applying the different assumptions mentioned above and assuming the vertical hydrostatic profile, with the integrations on the wet section $A_i(x,t) = b_i h_i(x,t)$ on the longitudinal Navier-Stokes component, the one-dimensional dynamic equations of flows, the new equation, which is the equation of Saint-Venant 1D, is given by [29], [30], [31] :

$$\begin{cases} b_i \frac{\partial h_i(x,t)}{\partial t} + \frac{\partial Q_i(x,t)}{\partial x} = q_{l,i}(x,t) \\ \frac{\partial Q_i(x,t)}{\partial t} + b_i \frac{\partial}{\partial x}\left[\frac{Q_i^2(x,t)}{h_i(x,t)}\right] + g b_i h_i(x,t) \frac{\partial h_i(x,t)}{\partial x} = k' \end{cases} \quad (6)$$

with,

$$k' = g b_i h_i(x,t)\left(S_0 - S_{f,i}\right) + q_{l,i}(x,t) v_{l,i}(x,t) \quad (7)$$

Considering the negligible contributions along the channels of the STHMD, a conservative form of equation (6) becomes:

$$\begin{cases} \frac{\partial h_i(x,t)}{\partial t} + \frac{1}{b_i}\frac{\partial Q_i(x,t)}{\partial x} = 0 \\ \frac{\partial Q_i(x,t)}{\partial t} + b_i \frac{\partial}{\partial x}\left[\frac{Q_i^2(x,t)}{h_i(x,t)}\right] + g b_i h_i(x,t) \frac{\partial h_i(x,t)}{\partial x} = k'' \end{cases} \quad (8)$$

with,

$$k'' = g b_i h_i(x,t)\left(S_0 - S_{f,i}\right) \quad (9)$$

As elucidated above, the equation (8) ensures that any change in the channel flow rate is compensated by a corresponding variation in the water section or its size. The second part allows the water-level profile to be followed and the flow rate to be recovered, thereby determining the speed in each channel. Knowing that, the following relation gives the flow rate per channel:

$$Q_i(x,t) = A_i(x,t).v_i(x,t) \quad (10)$$

The equation (8) can be expressed as a function of water flow speed and height using equation (10):

$$\begin{cases} \frac{\partial h_i(x,t)}{\partial t} + \frac{\partial}{\partial x}\left[h_i(x,t).V_i(x,t)\right] = 0 \\ \frac{\partial}{\partial t}\left[h_i(x,t).V_i(x,t)\right] + b_i^2 \frac{\partial}{\partial x}\left[h_i(x,t).V_i^2(x,t)\right] + g h_i(x,t) \frac{\partial h_i(x,t)}{\partial x} = k''' \end{cases} \quad (11)$$

with,

$$k''' = g h_i(x,t)\left(S_{f,i} - S_0\right) \quad (12)$$

These relations directly link flow speed to water height in the channel. For each water depth value, these relations allow the velocity profile along the channel to be determined. This height also varies with the period of floods or storms. Thus, for each channel, the following equations are:

- For channel $i = 1$ :

$$\begin{cases} \frac{\partial h_1(x,t)}{\partial t} + \frac{\partial}{\partial x}\left[h_1(x,t).V_1(x,t)\right] = 0 \\ \frac{\partial}{\partial t}\left[h_1(x,t).V_1(x,t)\right] + b_1^2 \frac{\partial}{\partial x}\left[h_1(x,t).V_1^2(x,t)\right] + g h_1(x,t) \frac{\partial h_1(x,t)}{\partial x} = k_1'''' \end{cases} \quad (13)$$

with,

$$k_1'''' = g h_1(x,t)\left(S_{f,1} - S_0\right) \quad (14)$$

- For channel $i = 2$ :

$$\begin{cases} \frac{\partial h_2(x,t)}{\partial t} + \frac{\partial}{\partial x}[h_2(x,t).V_2(x,t)] = 0 \\ \frac{\partial}{\partial t}[h_2(x,t).V_2(x,t)] + b_2^2 \frac{\partial}{\partial x}[h_2(x,t).V_2^2(x,t)] + gh_2(x,t)\frac{\partial h_2(x,t)}{\partial x} = k_2'''' \end{cases} \quad (15)$$

with,

$$k_2'''' = gh_2(x,t)\left(S_{f,2} - S_0\right) \quad (16)$$

The geometric configuration of the two channels being identical and the two channels being placed in the bed of the river, thus connected to the same upstream basin and to the same downstream, it is admitted that the dynamic parameters are identical; therefore, the free surface condition is established:

$$h_1(x,t) = h_1(x,t) = h(x,t) \quad (17)$$

$$Q_{tc}(x,t) = Q(x,t) + Q_S(t) \quad (18)$$

where: $Q_{tc}(x,t)$ is the total flow during floods, $Q_s(x,t)$is the additional flow through the spillway (submersible threshold) during floods, and $Q(x,t)$ is the channel set-aside. In the absence of floods, the flow $Q_{tc}(x,t)$ is assumed to be zero; because all the load is concentrated on the channels, the necessary flow, noted as measured flow, can be written:

$$\begin{cases} \frac{\partial}{\partial x}[h_1(x,t).V_1(x,t)] = 0 \\ b_1^2 \frac{\partial}{\partial x}[h_1(x,t).V_1^2(x,t)] + gh_1(x,t)\frac{\partial h_1(x,t)}{\partial x} = k_1'''' \end{cases} \quad (19)$$

From the equation (19), the upper part shows that the flow rate becomes constant, implying that the discharge remains constant along the channel. This reflects a conservative flow, with neither lateral inflow nor outflow. Based on this result, the equation of gradually varied flow profiles at the level of the flows is given by the relation (20) [32], [33] :

$$\frac{dh_i}{dx} = \frac{S_0 - S_{f,i}(h_i)}{1 - F_r^2(h_i)} \quad (20)$$

This relationship (20) allows for the analysis of the flow speed profile or speed field as a function of water height, where $S_f$ and $Fr$ are respectively the friction slope and the Froude number given by the expressions depending on the depth of water in the rectangular channels:

$$S_{f,i}(h_i) = n^2 \frac{Q_i^2}{(b_i h_i)^2}\left(\frac{b_i h_i}{b_i + 2h_i}\right)^{-4/3} \quad (21)$$

$$F_{r,i}(h_i) = n^2 \frac{Q_i^2}{(b_i h_i)^2}(b_i h_i)^{-1/2} \quad (22)$$

Generally, for Froude numbers near unity, flow in inclined channels can be characterized as critical, supercritical, or too fast; in the latter case, the regime a subcritical. This value enables analysis of the fluid speed at the channel outlets.

## Determination of flow parameters in the channels

Sizing studies of hydraulic structures with channels are generally carried out in a steady-state, uniform regime, which a still relatively uncommon in practice but is crucial because it allows analytically determining the hydrodynamic values at the channel level. In this context,

the geometric quantities no longer vary with the flow direction and remain constant over time. Within the studied network, the flow rate, water depth, and wet section remain constant throughout the channels. However, the flow remains turbulent due to local random fluctuations in the water, while the overall dynamics remain stable. Therefore, it is noted that the slopes $S_f$ and $S_0$ are equal. For permanent, uniform flows, the Manning-Strickler formulation is used to determine specific quantities for free-surface flows. For uncovered rectangular channels $i(i = 1,2)$ in smooth concrete, the channel roughness (Manning coefficient) n is generally low but not negligible [34], [35]. Different parameters are determined:

- Flow speed at each channel

Knowing in the context of the studied network, the width of the channels is not significantly greater; the following relationship can determine the water flow speed at the level of the micro-dam channels:

$$V_i = \frac{1}{n}\left(\frac{b_i h_i}{b_i+2h_i}\right)^{2/3} \cdot \sqrt{S_0} \tag{23}$$

- Flow rate for each channel

$$Q_i = \frac{1}{n} b_i h_i \left(\frac{b_i h_i}{b_i+2h_i}\right)^{2/3} \cdot S_o^{1/2} \tag{24}$$

This equation also enables the determination of the bottom slope (friction slope) as a function of the flow rate.

- Pressure losses in the channel

The losses in the channels of the hydraulic micro-dam with a submersible threshold are due to friction during the flow of fluid (water) along the channel of length $L$ and by singularity (control valve, protective gray, etc.).

The friction losses, also called distributed losses $h_{f,distributed}$ (m) are modelled by the Manning formulation:

$$h_{f,distributed} = n^2 L_i V_i^2 \left(\frac{b_i h_i}{b_i+2h_i}\right)^{-4/3} \tag{25}$$

The singular losses at the channel level, also called local losses, noted $h_{loc,i}$ are measured by the following relationship:

$$h_{loc,i} = K\frac{V_i^2}{2g} \tag{26}$$

where: K represents the specific coefficient of the singularity, with $j(j = 1,2,\dots)$, the number of singularities.

By summing equations (25) and (26), one can easily deduce the total losses for each channel by the following relation:

$$h_f = K\frac{V_i^2}{2g} + n^2 L_i V_i^2 \left(\frac{b_i h_i}{b_i+2h_i}\right)^{-4/3} \tag{27}$$

- Hydraulic power for each channel

The two-channel submersible threshold micro-dam allows for a partial retention of the flow required to drive turbines by optimizing channel slope, thereby increasing flow speed. The difference in heights noted $H_{u,i}$ between the upstream and downstream of the channels makes it possible to estimate the hydraulic power in each channel after substitution of losses by the following relationship [36] :

$$P_{h,i} = \rho g Q_i H_{u,i} \tag{28}$$

where: $H_{u,i}$ is the proper height between the water intake point and the channel outlet point. Given the relationship between specific energy and channel depth, the useful power is written as a function of local losses (grid and valve) and specific energy. This difference constitutes the useful hydraulic load:

$$P_{h,i} = \rho g Q_i \left[h_i + (1-K)\frac{V_i^2}{2g}\right] \tag{29}$$

**Modelling of the spill: Submersible threshold**

In the context of the studied micro-dam, the submersible threshold is a spillway. It is constructed of smooth concrete and is directly integrated into the riverbed. In this configuration, the threshold regulates the upstream level and flow rate, thereby maintaining a sufficient hydraulic load to supply the two flow channels leading to the crossflow turbines. The modelling of the threshold is generally done for a normal exploitation, in a free flow (non-submerged) regime according to KINDSVATER and CARTER (1957) [37] by the following relation:

$$Q_S = C_d B \sqrt{2g} H_1^{3/2} \tag{30}$$

where: $C_d$ represents the coefficient of the large peak spillway. For our study, the submersible threshold is designed for free-flow baseflow; however, temporary flooding during flood periods is normal and acceptable. In the event of temporary flooding, for a few hours or days, the downstream level rises to $H_2$.The regime then becomes half-free until the excess flow is evacuated and $H_2$ falls back, according to equation (30) associated with the coefficient of Brater and King (1976). Thus, the threshold is modelled by:

$$Q_{S,Cr} = C_d B \sqrt{2g} H_1^{3/2} \left[1 - \left(\frac{H_2}{H_1}\right)^{3/2}\right]^{0,385} \tag{31}$$

where: $Q_{s,Cr}$ represents the flow rate at the level of the submersible threshold during temporal floods. This relationship enables a thorough analysis of the influence of floods on the spillway, which can reduce the available payload.

**Determination of the Reynolds number and flow regime**

To characterize the flow regime within micro-dam channels, the Reynolds number (Re) is commonly evaluated using the channel height and flow velocity. This dimensionless parameter provides essential insight into the nature of the flow and allows distinguishing between laminar, transitional, and turbulent regimes. Its determination is also necessary to justify the choice of the turbulence modelling approach adopted in analytical equations and in numerical simulations. It is calculated by the following equation (32) [38], [39] :

$$R_e = \rho \frac{V_i D_{h_i}}{\mu} \tag{32}$$

where: $D_{h_i}$ is the hydraulic diameter of the channel (m).

## Two-dimensional numerical modelling using COMSOL Multiphysics

The 2D numerical simulation was performed in COMSOL Multiphysics to validate the analytical model. Using the analytical approach, the 1D model assumed a permanent, uniform, gradually varied flow with an average speed distribution. The numerical model implemented enables the analysis of complex spatial effects, including turbulence, recirculation zones, and localized energy losses at the channel level, with high precision. Unlike unidirectional modelling, in which the flow is assumed to be uniform over the entire section, a 2D simulation was performed, enabling the resolution of 2D equations and the capture of spatial variations in velocity and pressure fields for equations (3) and (4). This simulation provides a complete representation of speed, pressure, and turbulence fields at the channel level, along with their associated values.

The STHMD numerical model was developed in 2D using the COMSOL Multiphysics environment for steady-state simulation (Figure 9). It consists of a river, a dam, and a concrete flow channel with a free water surface exposed to the atmosphere, with negligible inflows. The boundary conditions applied to the model are as follows: the inlet boundary conditions have a prescribed uniform flow speed corresponding to the measured river flow $V_0 = 0.297\ m.s^{-1}$ on site. The outlet boundary is defined with a fixed atmospheric pressure.

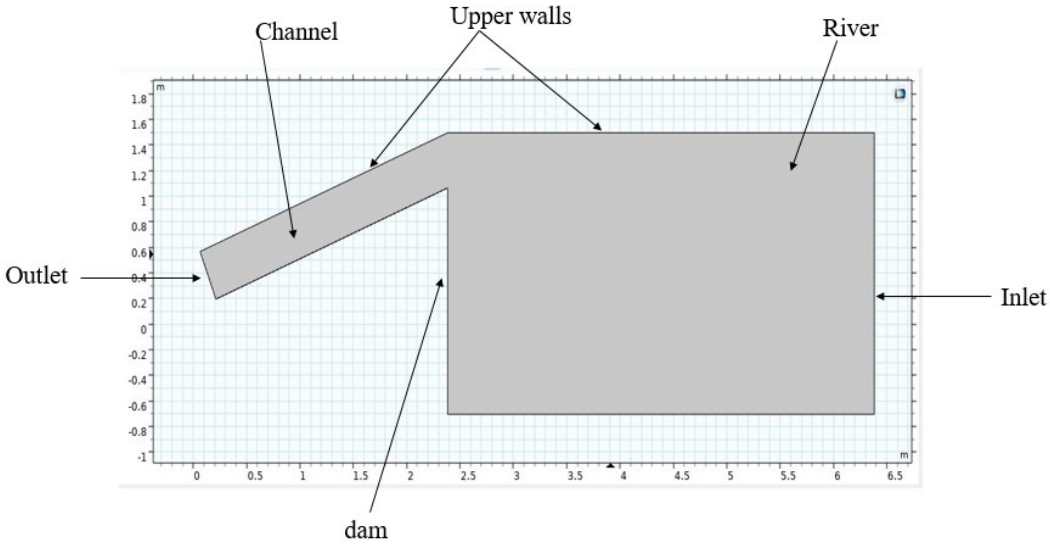


Figure 9. Two-dimensional numerical domain of the STHMD in COMSOL Multiphysics showing boundary conditions.

The upper boundary representing the free water surface is modeled using a symmetry condition, which imposes zero velocity ($V \cdot n = 0$) and zero tangential shear stress ($\tau = 0$). This condition prevents any fluid flux across the free surface while allowing unrestricted tangential flow, thereby correctly representing the physical behavior of an open-channel free surface in a single-phase flow simulation.

The flow is modeled using the Reynolds-averaged form of the Navier-Stokes (RANS) equations, coupled and solved using the Shear Stress Transport (SST) turbulence model. The SST turbulence model was adopted because it combines the near-wall accuracy of the k–ω formulation with the robustness of the k–ε formulation in the free stream, making it particularly suitable for separated and highly sheared flows. Some studies show that three-dimensional models can correct the overestimates of energy and shear typical of unidirectional models [40]. A two-dimensional representation of the micro-dam and its channels was adopted for the

numerical simulation. Although three-dimensional simulations can provide more detailed insights. Figure 10 below shows the extremely fine-meshed (Figure 10.a) and the fine-meshed (Figure 10.b) of the two-dimensional model.

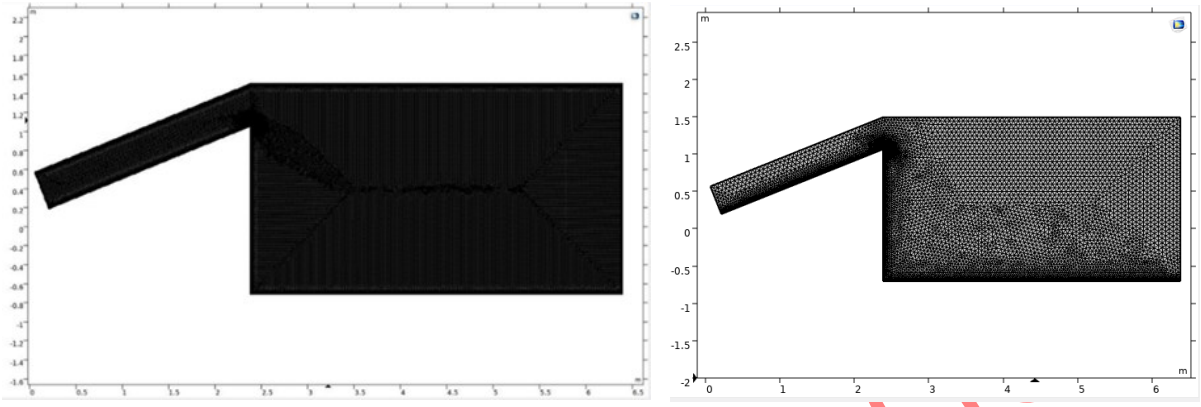

(a) (b)

Figure 10. Presentation of the extremely fine mesh (a) and the fine mesh (b) of the two-dimensional model of the micro-dam with a submersible threshold.

The full 3D simulations are significantly more computationally demanding and can be difficult to manage for realistic geometries and complex flow configurations. This work is limited to 2D simulations to maintain computational feasibility and keep the analysis tractable. The extremely fine meshed was adopted for the simulations.

## RESULTS AND DISCUSSION

This section presents the results obtained from the analytical model and the two-dimensional COMSOL numerical simulations, followed by a comparative discussion of both approaches.

### Unidirectional simulations of the flow in channels

The raw river data do not support the development of significant, stable hydroelectric power due to fluctuations in rivers in rural communities (flow rate, speed, and level). The installation of a submersible threshold hydraulic micro-dam increases flow speed and stabilizes flow. The general data of the micro-dam are included in the following Table 2:

**Table 2.** Geometric characteristics of the studied network and parameters used

| Variables | Symbol | Unit | Values |
|---|---|---|---|
| Length of the channel | L | m | 2.7 |
| Width of the channel | b | m | 0.6 |
| Exploitable channel height | $h_{exp}$ | m | 0.45 |
| Channel bottom slope | $S_o$ | (° or %) | 40%/21.8° |
| Cross section | $S_t$ | $m^2$ | 0.48 |
| Upstream channel height | $H_{am}$ | m | 1.75 |
| Downstream channel height | $H_{av}$ | m | 0.75 |
| Net useful drop height | $H_u$ | m | 1 |
| Threshold height | $H_s$ | m | 2.2 |

| Variables | Symbol | Unit | Values |
|---|---|---|---|
| Threshold width | B | m | 2.6 |
| Dam length | $L_b$ | m | 7.5 |
| Height dam zone channels | $H_b$ | m | 2.67 |
| Manning coefficient | n | - | 0.03 |
| Coefficient of singular losses | K | - | 0.2 |
| Density of water | ρ | $Kg/m^3$ | 1000 |
| Gravitational acceleration | g | $m.s^2$ | 9.81 |
| Dynamic viscosity | μ | Pa.s | $1.0x10^{-3}$ |

The previously integrated Saint-Venant equations have been solved numerically in the framework of a uniform and gradually varied permanent flow, allowing us to the main hydraulic parameters along the rectangular channels. The analytical calculations were performed in Excel using an interactive model that included analytical formulas for the sections and hydraulic quantities. For these calculations, the above parameters were carefully considered during the micro-dam's design to ensure realism. Table 3 below shows the values and hydraulic power per channel, rounded to $10^{-2}$, for water depths ranging from 0.1m to 0.20m.

**Table 3.** Hydraulic speeds and powers per STHMD channel.

| Depth (h=y) | Mean flow Speed per channel (m/s) | Maximum speed per channel (m/s) | Theoretical hydraulic power per channel (kW) |
|---|---|---|---|
| 0.10 | 9.82 | 10.80 | 28.96 |
| 0.11 | 8.92 | 9.82 | 24.09 |
| 0.12 | 8.18 | 9.00 | 20.40 |
| 0.13 | 7.55 | 8.31 | 17.54 |
| 0.14 | 7.01 | 7.71 | 15.29 |
| 0.15 | 6.54 | 7.20 | 13.48 |
| 0.16 | 6.14 | 6.75 | 12.01 |
| 0.17 | 5.77 | 6.35 | 10.80 |
| 0.18 | 5.45 | 6.00 | 9.80 |
| 0.19 | 5.17 | 5.68 | 8.96 |
| 0.20 | 4.91 | 5.40 | 8.25 |
| 0.21 | 4.67 | 5.14 | 7.65 |
| 0.22 | 4.46 | 4.91 | 7.13 |

This allowed us to obtain the speed figures, the Froude number, the useful hydraulic power and the profile of the water line in the channels. The Figure 11, Figure 12, Figure 13 and Figure 14, present the simulation results given by the following curves:

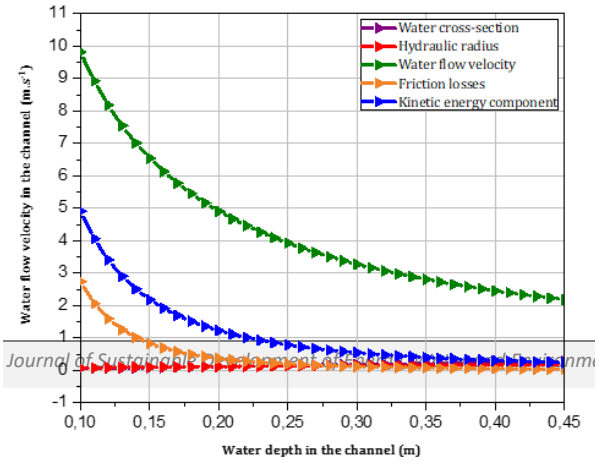


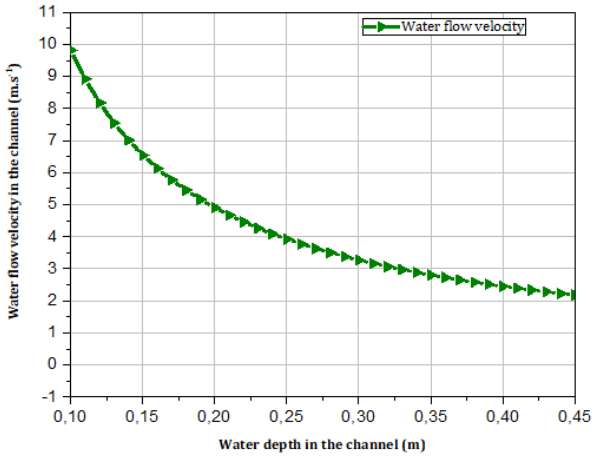

Figure 11. Water flow speed in the channel ($m.s^{-1}$)

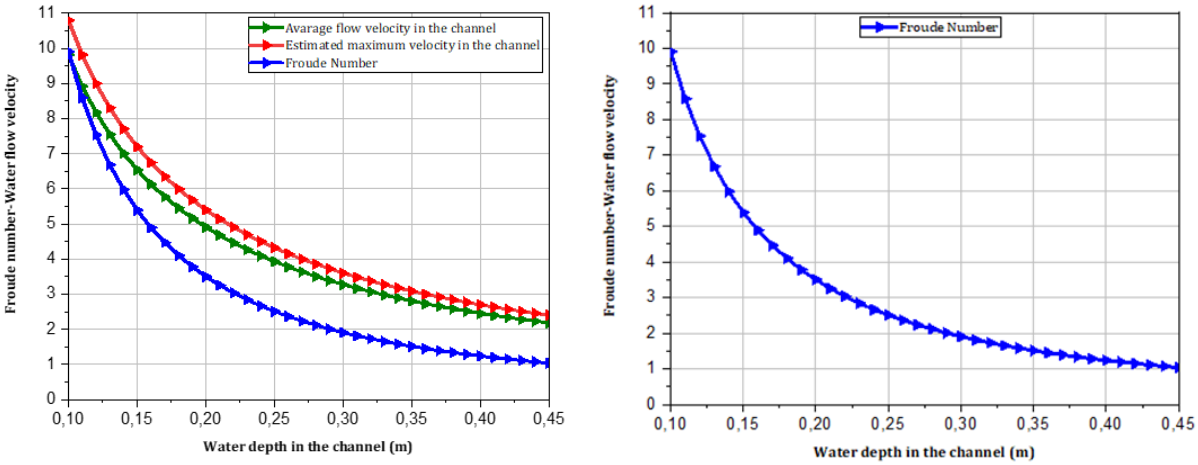


Figure 12. The Froude number depends on the channel's water depth.

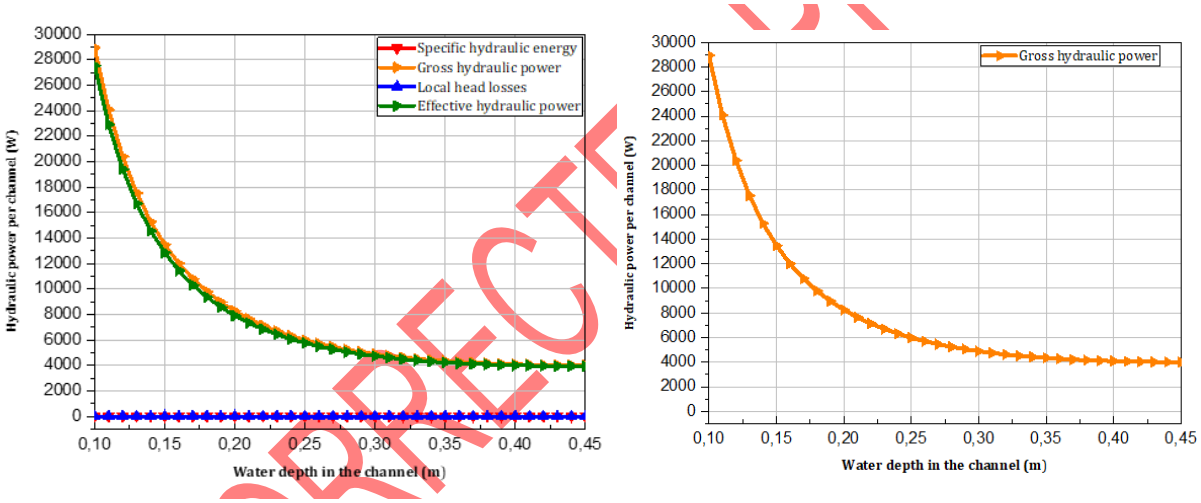


Figure 13. Theoretical hydraulic power according to the depth of a channel

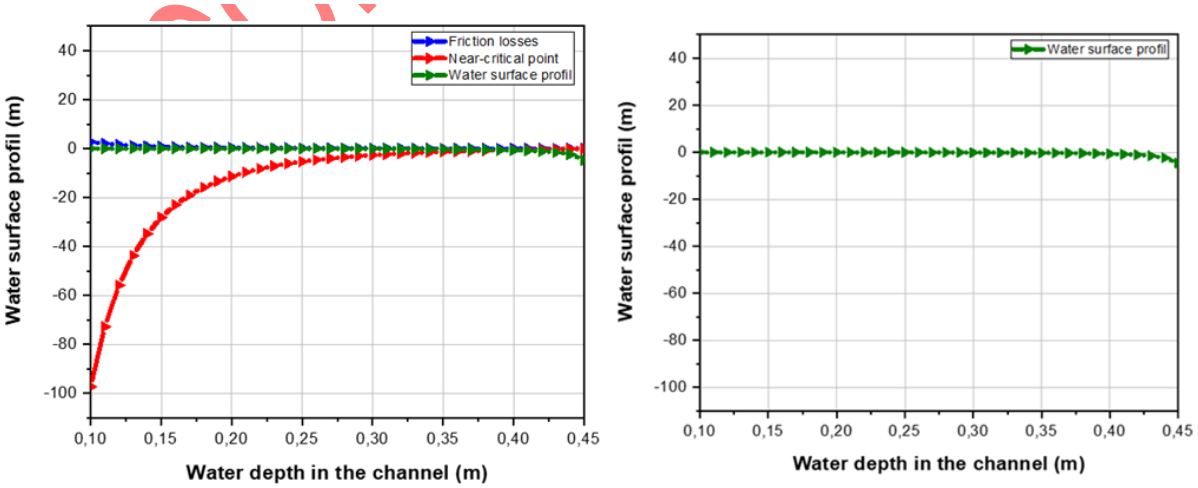


Figure 14. Water surface profile in a channel (m)

Based on the studied conditions, Table 4 represents the results of Reynold number with the main values of water depth and flow speed in the channel:

**Table 4.** Reynolds number and flow regime

| Depth (h) | Hydraulic Diameter of the channel (m) | Mean speed analytical results (m/s) | Reynolds number ($x10^5$) |
|---|---|---|---|
| 0.10 | 0.150 | 9.82 | 14.72 |
| 0.15 | 0.200 | 6.54 | 13.08 |
| 0.20 | 0.240 | 4.91 | 11.78 |
| 0.25 | 0.273 | 3.93 | 10.70 |
| 0.30 | 0.300 | 3.27 | 9.82 |
| 0.35 | 0.323 | 2.80 | 9.06 |
| 0.40 | 0.343 | 2.45 | 8.41 |
| 0.45 | 0.360 | 2.18 | 7.85 |

For all depths in the channel, the Reynolds number ranges from approximately $7.8x10^5$ to $14.72x10^5$, confirming fully turbulent ( Re 4000 ) flow conditions throughout. This result is physically consistent with the conservation of flow rate. Indeed, as water depth increases, the mean flow speed decreases proportionally, and the Reynolds number decreases accordingly. This confirms the suitability of the turbulent regime for the analytical approach and of the Reynolds-averaged Navier-Stokes (RANS) equations.

**Unidirectional analysis and discussion**

Calculations based on the integrated equations for the studied model enabled the determination of the main hydraulic and energy parameters as a function of water depth varying between 0.10m and 0.45m. The results show a consistent evolution of speed, Froude number, head loss, and hydraulic power across the study area. The critical depths translate the local trend of the flow profile. It is observed that below the critical depth, the flow is supercritical; beyond it, the slope becomes weakly positive, confirming a gradually varied, stable flow. The specific head losses are low relative to the channels' geometric slope, which supports the validity of the quasi-permanent flow assumption adopted in this study. The curve indicates a marked decrease in average speed with increasing water depth in the channels. For water depths of 0.10-0.22 m, mean flow speeds of 4.46-9.82 m/s per channel are observed, corresponding to velocity amplification of approximately 15-33 times the initial river velocity of 0.297 m/s. This acceleration confirms the STHMD's ability to generate supercritical flow conditions suitable for driving crossflow turbines. Therefore, reliable hydroelectric production is achieved [41]. This configuration enabled the theoretical hydraulic power range of 14.26-57.92 kW. After taking into account the local losses due to the singular losses caused by the grids (trash racks) and control valves, the net hydraulic powers, which are significant, decrease from 55.08 kW to 13.68 kW between 0.10m and 0.22m for both channels, representing a reduction in losses to 4.9% and therefore a hydraulic efficiency of 95.1%. This result confirms the approach that, for hydraulic micro-dam systems used for hydroelectricity, limiting head losses to 5% of the net head height is a good sizing rule. The pressure losses at the channel level in the model studied account for almost half of the indicated percentage; they are low but not negligible, as for low-

power run-of-river structures, a rigorous estimation of losses is essential to ensure reliable production [42], [43]. The other observation is that outside this interval, the theoretical power gradually decreases until it reaches a stable value of approximately 7.86 kW (starting from 0.45m); this pattern is the same as that observed at the speed level. The results of our model confirm the validity of the 1D Saint-Venant model for a hydraulic micro-dam channel with a submersible threshold. Still, it remains overestimated in the absence of three-dimensional effects. Therefore, in this study, a validation using two-dimensional modelling in COMSOL Multiphysics is necessary to refine the parameter distribution.

## Two-dimensional analysis and discussion

The 2D simulation, combined with the SST turbulence model and fine meshing, provides accurate predictions of speed and pressure, sufficient to validate the analytical model and assess hydraulic performance. The simulation of flows was carried out according to the water level in the channels with a step of 0.05m to limit the images, unlike the step chosen with analytical calculations, which allowed obtaining the following speed and pressure fields for the flow levels $h$ (0.10m, 0.15m, 0.20m, 0.25m, 0.30m, 0.35m, 0.40m et 0.45m) in Figure 15 bellow :

- $h = 0.10m$

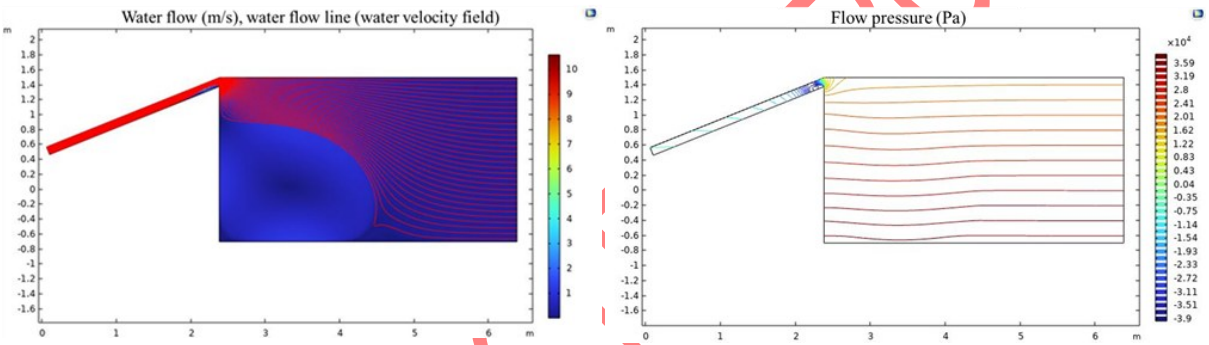


- $h = 0.15m$

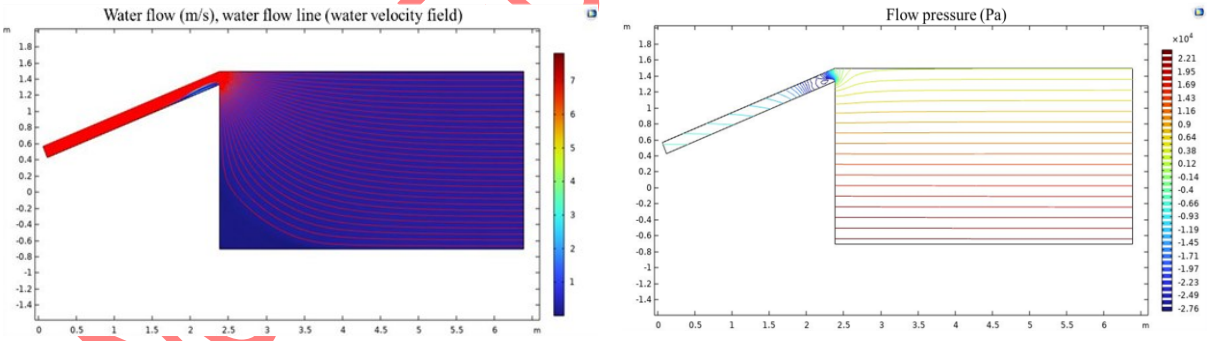


- $h = 0.20m$

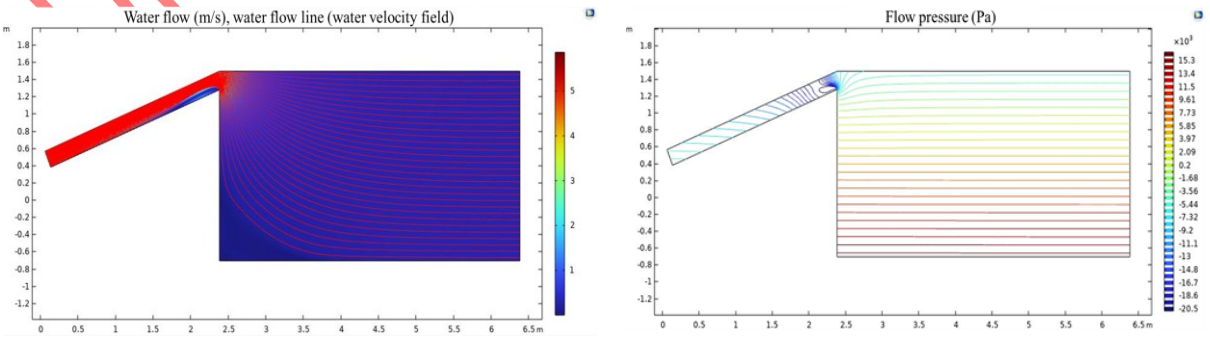

- $h = 0.25m$

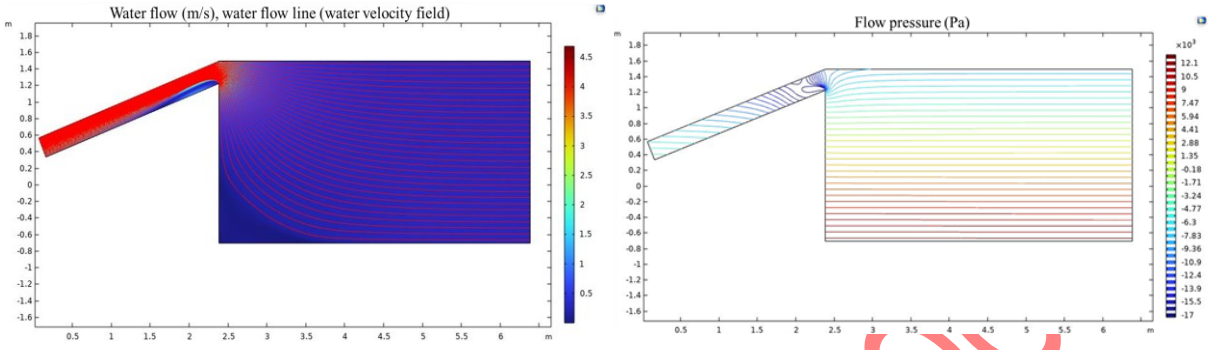


- $h = 0.30m$

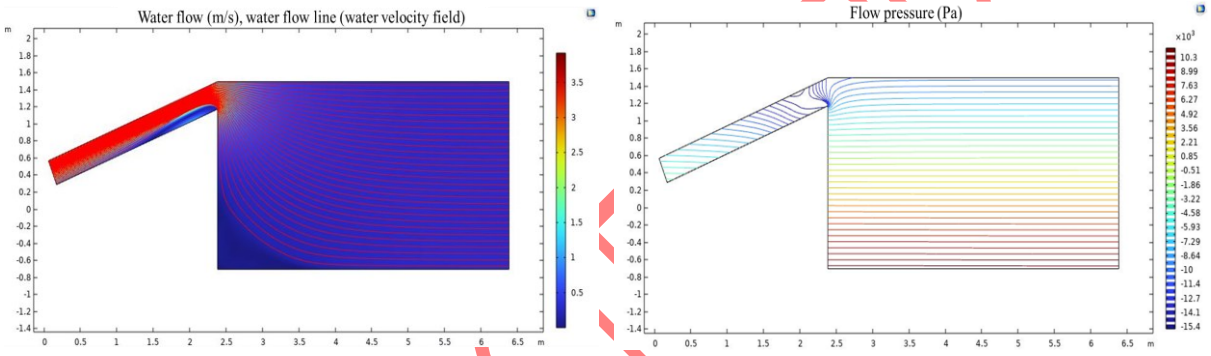


- $h = 0.35m$

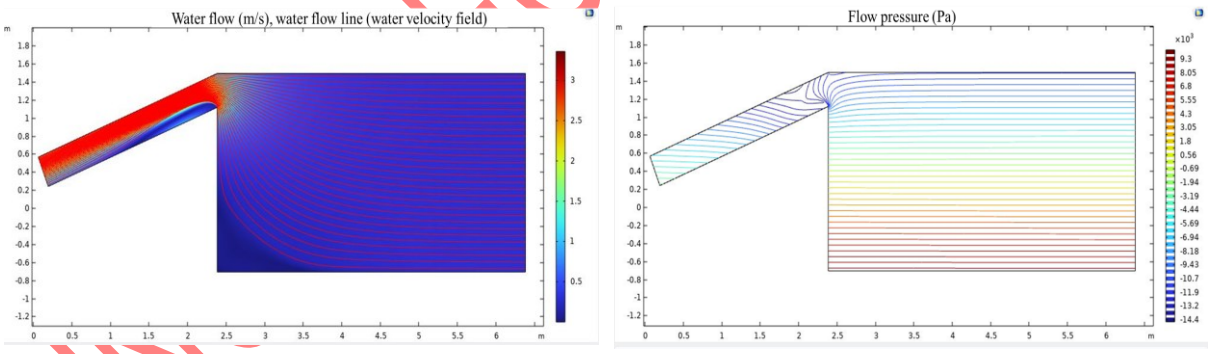


- $h = 0.40m$

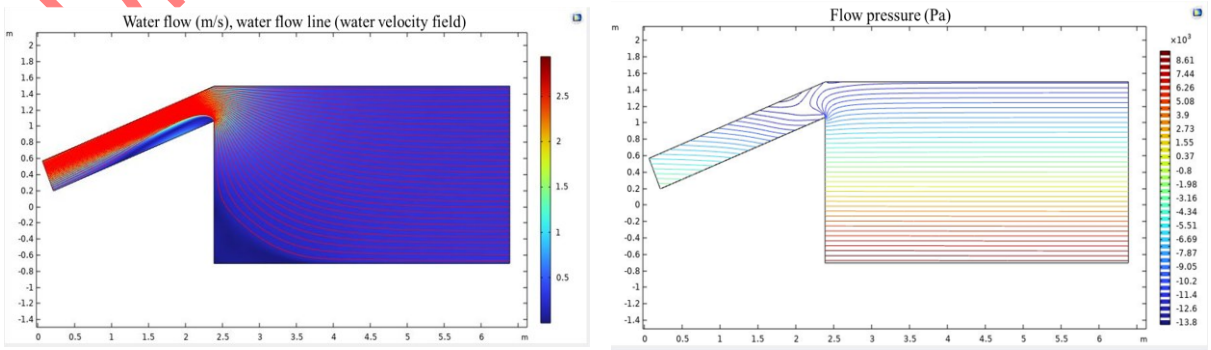

- $h = 0.45m$

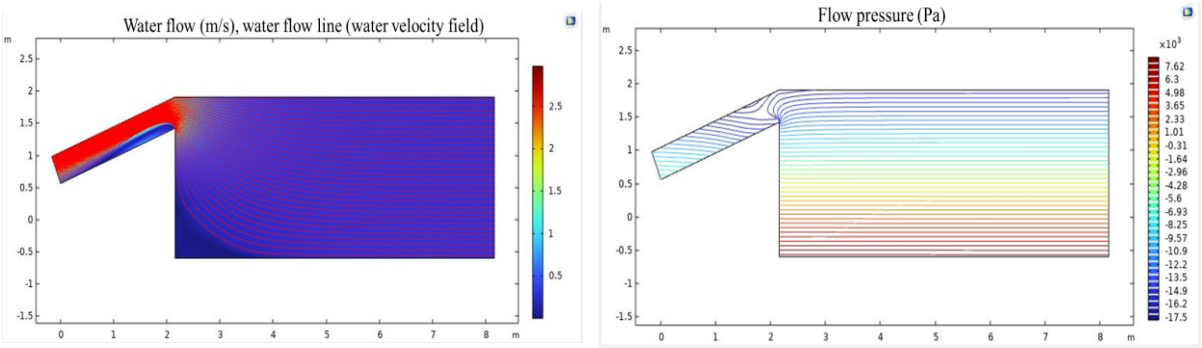


Figure 15. Two-dimensional velocity fied (m/s) and Two dimensional pressure field (Pa) simulated in COMSOL Multiphysics for different flow height h(m) per channel.

The results from analytical modelling and CFD-2D simulations using COMSOL Multiphysics demonstrate satisfactory overall consistency for the average flow velocities and pressures in the micro-dam channels at the submersible threshold. Figure 15 indicates that the simulated velocities are very close to the analytical ranges across all channel depths when a step size of 0.05m is used, with an average relative error of less than 5%, confirming the validity of the theoretical model based on the Saint-Venant integrated equations. For the maximum water height in the channel ( $h = 0.45m$ ), the simulated average speed differs by only 12.8% compared to numerical calculations. This difference gradually decreases with increasing channel depth, reflecting a convergence of models in faster flow regimes. Relative differences of 6.57% and 1.80%, respectively, in the heights of 0.30m and 0.10m were observed **[34]**. These discrepancies are explained by the approximations introduced in the unidimensional formulation, a hypothesis on permanent and uniform flow, which tend to neglect the three-dimensional effects of turbulence (here observed at the entrance of the channels) and shear stresses near the walls, captured by CFD models; the simulation also shows a quasi-linear increase in pressure with the reduction of water height, from 7.62 kPa to 30.19 kPa respectively for heights 0.45m and 0.10m [44]. This trend reflects the progressive conversion of potential energy into negative energy as the wet section decreases and speed increases. The numerical results, therefore, confirm the expected behaviour of a gradually varied flow at high slope and validate the assumptions used and the hydrodynamic consistency of the analytical modelling, thereby establishing the relevance of the method for refining the distribution of velocities and pressures in the channels of the submersible threshold hydraulic micro-dam. Table 5, following, confirms the validation of the analytical model by comparing the speed results of the Figure 9 with the numerical approach, through the extraction speed from the COMSOL results:

**Table 5.** Speed analytical results vs speed COMSOL numerical results

| Depth (h) | Mean speed analytical results (m/s) | Speed from COMSOL results (m/s) | Gap speed (%) |
|---|---|---|---|
| 0.10 | 9.82 | 10.00 | 1.80 |
| 0.15 | 6.54 | 7.00 | 6.57 |

| Depth (h) | Mean speed analytical results (m/s) | Speed from COMSOL results (m/s) | Gap speed (%) |
|---|---|---|---|
| 0.20 | 4.91 | 5.00 | 1.80 |
| 0.25 | 3.93 | 4.50 | 12.66 |
| 0.30 | 3.27 | 3.50 | 6.57 |
| 0.35 | 2.80 | 3.00 | 6.66 |
| 0.40 | 2.45 | 2.50 | 2.00 |
| 0.45 | 2.18 | 2.50 | 12.8 |

A comparison between the analytical model based on the Saint-Venant equations and the numerical results obtained using COMSOL Multiphysics was carried out for different water depths. The results in Table 4 show a good overall agreement between the two approaches, as shown in Figure 16. The relative deviation in flow speed remains low, generally below 10%, with most values ranging from 1.8% to 6%. This confirms the analytical model's ability to accurately predict the mean flow behaviour in the channel.

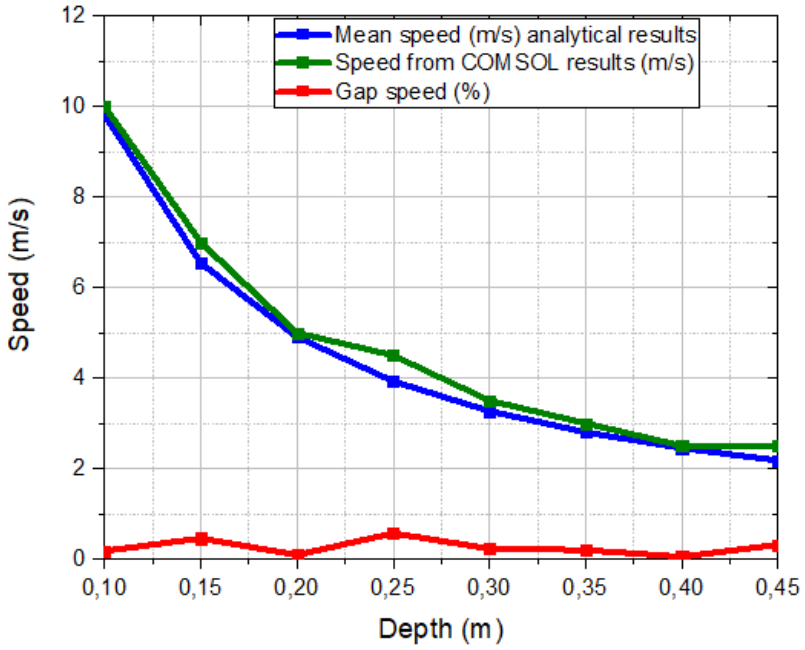


Figure 16. Comparison of analytical and numerical approaches results

At lower water depths ( $h = 0.10 - 0.20m$ ), as shown in Figure 16, the variation remains very small (arround 1.8%-6.6%), indicating that the simplified analytical model captures the dominant flow physics well under shallow flow conditions. However, for the intermediate depths ( $h = 0.25m$ and $h = 0.45m$ ), slightly higher discrepancies are observed (up to approximately 12%). These differences can be attributed to the increasing influence of complex flow phenomena such as turbulence, recirculation zones, and two-dimensional effects, which are not fully captured by the one-dimensional analytical formulation but are resolved in the numerical model. Despite these localized differences, the global trend of velocity variation with water depth is consistently reproduced by both approaches. The analytical model correctly predicts the inverse relationship between flow depth and speed, as confirmed by the numerical simulation. These results demonstrate that the analytical model provides a reliable and efficient tool for preliminary design and engineering estimation of flow characteristics in the proposed micro-dam configuration.

## CONCLUSIONS

In this study, the methodological approach made it possible to model, design, and analyze the behaviour of the hydrodynamic flows of a submersible threshold micro-dam intended for electricity production, based on the Saint-Venant integrated equations, and a 2D numerical simulation under COMSOL Multiphysics, to validate the theoretical results of the flow in the channels. Analytical calculations enabled the determination of the speed profiles, Froude numbers, load losses, and useful hydraulic power for water depths ranging from 0.10 m to 0.45 m. It has been shown that the average speeds in each channel range from 2.18 m/s to 9.82 m/s, depending on the height of the water column, corresponding to supercritical flow at shallow depths and subcritical flow at water depths approaching 0.45 m. The theoretical hydraulic power per channel is approximately 28.96 kW, yielding an estimated total of 57.92 kW across the two parallel channels, confirming the device's energy potential. The results of the numerical simulation showed a very good agreement with the analytical values, with an average error of 4.03% on the speeds. The simulated pressures, ranging from 7.62 kPa to 30.19 kPa, reflect the gradual convergence of potential energy, while the velocity field distribution supports the validity of the gradually varied flow hypothesis. These results demonstrate the model's physical consistency and the relevance of combining an analytical approach with numerical simulation for the design of small-scale hydraulic structures. Compared to micro-dams with diversion channels and penstocks, whose application is generally limited to sites with high head, the proposed STHMD enables electricity generation from small rivers with very low or nearly zero natural head in rural communities. Methodologically, this study combines a simplified model based on the 1D Saint-Venant equations with a 2D numerical simulation using COMSOL Multiphysics to validate flow distributions, speed, and hydraulic power in a low-fall river context. This approach explicitly addresses the short, double-channel configuration, with a submersible threshold placed directly in the river, a configuration underrepresented in the literature. This work demonstrates the potential of STHMD as a sustainable, low-cost solution for rural electrification in sub-Saharan Africa, particularly for rivers that cannot be diverted conventionally due to geomorphological constraints. The study provides practical guidelines for designing integrated hydraulic-hydroelectric micro-dams suitable for rural communities with minimal natural slope and limited hydraulic heads.



## ACKNOWLEDGMENTS

The authors would like to express their gratitude to Centre d'Excellence d'Oyo (CEO) for Renewable Energy and Energy Efficiency, at Oyo in Congo, for the data that made this study possible. They would also like to thank the funding provider for the publication of this work.

## REFERENCES

[1] Africa-EU Energy Partnership, 'Advancing Rural Electrification in Africa: Scaling Up Regulatory Best Practices to Accelerate Progress in Off-Grid Electrification', African Union, 2025. Accessed: Aug. 08, 2025. [Online]. Available: https://africa-eu-energy-partnership.org/

[2] Energy Capital & power, 'Hydropower Development and Investment Opportunities in the Republic of Congo', EU-AFRICA, Cape Town, South Africa, 2025. Accessed: Jul. 12, 2025. [Online]. Available: https://eu-africa-chamber.org/congo-energy-investment-forum-returns-to-brazzaville-in-march-2026

[3] International Hydropower Association, 'Global hydropower generation rebounds in 2024 and pumped storage development surges', IHA, 2025. Accessed: Aug. 09, 2025. [Online]. Available: https://www.hydropower.org/news/flagship-2025-world-hydropower-outlook-out-now

[4] International Hydropower Association, 'World hydropower Outlook', IHA, London, United Kingdom, 2025. Accessed: Aug. 09, 2025. [Online]. Available: https://www.rinnovabili.it/wp-content/uploads/2025/06/World-Hydropower-Outlook-2025-IHA.pdf

[5] A. Scotti, D. Jacobsen, and R. Bottarin, 'Small hydropower—Small ecological footprint? A multi-annual environmental impact analysis using aquatic macroinvertebrates as bioindicators. Part 2: Effects on functional diversity', *Front. Environ. Sci.*, vol. 10, p. 904547, Jul. 2022, doi: 10.3389/fenvs.2022.904547.

[6] D. Zhou and Z. (Daniel) Deng, 'Ultra-low-head hydroelectric technology: A review', *Renewable and Sustainable Energy Reviews*, vol. 78, pp. 23–30, Oct. 2017, doi: 10.1016/j.rser.2017.04.086.

[7] P. Punys, A. Dumbrauskas, A. Kvaraciejus, and G. Vyciene, 'Tools for Small Hydropower Plant Resource Planning and Development: A Review of Technology and Applications', *Energies*, vol. 4, no. 9, pp. 1258–1277, Aug. 2011, doi: 10.3390/en4091258.

[8] A. Barbón, F. González-González, L. Bayón, and R. Georgious, 'Variable-Speed Operation of Micro-Hydropower Plants in Irrigation Infrastructure: An Energy and Cost Analysis', *Applied Sciences*, vol. 13, no. 24, p. 13096, Dec. 2023, doi: 10.3390/app132413096.

[9] Y. T. Zerihun, 'On the Hydraulic Characteristics of Submerged Flow over Trapezoidal-Shaped Weirs', *Archives of Hydro-Engineering and Environmental Mechanics*, vol. 70, no. 1, pp. 1–16, Jan. 2023, doi: 10.2478/heem-2023-0001.

[10] F. M. Shehab and S. D. Jasim, 'Hydraulic Characteristics of Flow over Submerged Dams', *IOP Conf. Ser.: Mater. Sci. Eng.*, vol. 881, no. 1, p. 012037, Jul. 2020, doi: 10.1088/1757-899X/881/1/012037.

[11] V. J.R, 'Submerged-weir Discharge Studies', pp. 866–869, 1947.

[12] D. Kvočka, 'Two-dimensional hydraulic modelling of submerged river training structures', *Acta hydrotechnica*, pp. 79–96, Dec. 2020, doi: 10.15292/acta.hydro.2020.06.

[13] N. S. Ayoob and A. M. Hamad, 'Numerical Simulation for Flow over A Broad-Crested Weir Using FLOW-3D Program', *cea*, vol. 10, no. 5, pp. 2157–2171, Sep. 2022, doi: 10.13189/cea.2022.100534.

[14] A. Demirçelik, M. M. Duman, and E. İkincioğulları, 'Numerical Investigation of Flow Characteristics of Broad-Crested Weirs with Different Geometry', *IJERAD*, vol. 17, no. 1, pp. 247–256, Mar. 2025, doi: 10.29137/umagd.1519268.

[15] H. Rahimi *et al.*, 'Numerical Modelling of Turbulence Kinetic Energy in Open Channel Flows with Mixed-Layer Vegetation', *Water*, vol. 15, no. 14, p. 2544, Jul. 2023, doi: 10.3390/w15142544.

[16] J. B. Kodman, B. Singh, and M. Murugaiah, 'A Comprehensive Survey of Open-Source Tools for Computational Fluid Dynamics Analyses', *J. Adv. Res. Fluid Mech. Therm. Sc.*, vol. 119, no. 2, pp. 123–148, Jul. 2024, doi: 10.37934/arfmts.119.2.123148.

[17] E. Yulianti and E. Prasetyo, 'Optimization of the Weir as a Micro Hydro Power Plant in Bayang Nyalo Padang, West Sumatra', *SCBMEJ*, vol. 1, no. 4, p. 11, Aug. 2024, doi: 10.47134/scbmej.v1i4.3135.

[18] G. Gasore, A. Santos, E. Ntagwirumugara, and D. Zimmerle, 'Sizing of Small Hydropower Plants for Highly Variable Flows in Tropical Run-of-River Installations: A Case Study of the Sebeya River', *Energies*, vol. 16, no. 3, p. 1304, Jan. 2023, doi: 10.3390/en16031304.

[19] M. Mukhammadiyev, B. Urishev, E. Kan, and K. Juraev, 'New Methods of Application of Micro-Hydroelectric Power Plants at Existing Hydraulic Structures: Schemes, Parameters, Efficiency', *E3S Web Conf.*, vol. 320, p. 04009, 2021, doi: 10.1051/e3sconf/202132004009.

[20] S. Valentin, 'micro hydro power scout guide A Field Worker's manual Know how to Do, prepared by Dutch', Hydro Power, AMES-E/GTZ, German Partnership Energising Development Access to Modern Energy Services, GERMANY, 2009. Accessed: Aug. 20, 2025. [Online]. Available: https://energypedia.info/images/3/3b/Hydro_scout_guide_ET_may10.pdf

[21] R. B. Giarto, M. Kiptiah, and R. Pradana, 'Analysis of River Flow Velocity Using Current Meter with Six-Tenths Method and Two-Point Method (Case Study of Ampal River, Balikpapan City)', *IJRVOCAS*, vol. 3, no. 3, pp. 01–06, Dec. 2023, doi: 10.53893/ijrvocas.v3i3.212.

[22] M. Syaiful Alim, Arya Dewa Nugroho, Suyono Thamrin, and Rudy Laksmono4, 'Optimization of Micro Hydro Power Plants to Support Community Energy and Indonesian National Army Training in Gunung Halu, West Bandung Regency', *IJHESS*, vol. 3, no. 5, Apr. 2024, doi: 10.55227/ijhess.v3i5.994.

[23] S. O. Anaza, A. M. S., Y. Y. A., Y. Y. O., S. B. U., and M. S. U., 'Micro Hydro-Electric Energy Generation- An Overview', *American Journal of Engineering Research (AJER)*, vol. 6, no. 2, pp. 05–12, 2017.

[24] Masna, Tulus, and Sawal, 'Computational analysis dynamics fluid of flow in dam using COMSOL Multiphysics', *J. Phys.: Conf. Ser.*, vol. 2421, no. 1, p. 012047, Jan. 2023, doi: 10.1088/1742-6596/2421/1/012047.

[25] D.-C. Lo and Y.-S. Tsai, 'A 3D Fully Non-Hydrostatic Model for Free-Surface Flows with Complex Immersed Boundaries', *Water*, vol. 14, no. 23, p. 3803, Nov. 2022, doi: 10.3390/w14233803.

[26] U. Farooq, S. Li, and J. Yang, 'Numerical Analysis of Flow Characteristics and Energy Dissipation on Flat and Pooled Stepped Spillways', *Water*, vol. 16, no. 18, p. 2600, Sep. 2024, doi: 10.3390/w16182600.

[27] A. Ghaderi, S. Abbasi, and S. Di Francesco, 'Numerical Study on the Hydraulic Properties of Flow over Different Pooled Stepped Spillways', *Water*, vol. 13, no. 5, p. 710, Mar. 2021, doi: 10.3390/w13050710.

[28] A. Benavides-Morán, L. Rodríguez-Jaime, and S. Laín, 'Numerical Investigation of the Performance, Hydrodynamics, and Free-Surface Effects in Unsteady Flow of a Horizontal Axis Hydrokinetic Turbine', *Processes*, vol. 10, no. 1, p. 69, Dec. 2021, doi: 10.3390/pr10010069.

[29] S. Kane *et al.*, 'Modeling of Unsteady Flow through Junction in Rectangular Channels: Impact of Model Junction in the Downstream Channel Hydrograph', *CWEEE*, vol. 06, no. 03, pp. 304–319, 2017, doi: 10.4236/cweee.2017.63020.

[30] M. Ersoy, O. Lakkis, and P. Townsend, 'A Saint-Venant Model for Overland Flows with Precipitation and Recharge', *MCA*, vol. 26, no. 1, p. 1, Dec. 2020, doi: 10.3390/mca26010001.

[31] F. T. Namio and E. Ngondiep, 'Mathematical Model of Complete Shallow Water Problem with Source Terms, Stability Analysis of Lax-Wendroff Scheme', *J Theor Comput Sci*, vol. 02, no. 04, 2015, doi: 10.4172/2376-130X.1000132.

[32] D. Apsley, 'Open-Channel Flow: Gradually Varied Flow'. 2025. Accessed: Sep. 15, 2025. [Online]. Available: https://personalpages.manchester.ac.uk/staff/david.d.apsley/lectures/hydraulics3/OCFGvf.pdf

[33] D. DORCHIES, J.-P. AUBRY, M. CHOUET, and F. GRAND, 'Cassiopée software', UMR G-EAU, Ecohydraulics research and development center, Montpellier, France, version 4.19.0, Mar. 2025. Accessed: Sep. 15, 2025. [Online]. Available: https://cassiopee.g-eau.fr/assets/docs/pdf/cassiopee_doc_fr.pdf

[34] J. Wang, R. Qiu, X. Xia, X. Li, C. Zhang, and W. Wang, 'A Modified Manning's Equation for Estimating Flow Rate in Grass Swales under Low Inflow Rate Conditions', *Water*, vol. 16, no. 11, p. 1613, Jun. 2024, doi: 10.3390/w16111613.

[35] B. Achour and L. Amara, 'Proper relationship of manning's coefficient in a partially filled circular pipe', 2020.
[36] Rashi Sahay and Swamy Tn, 'Micro-Hydro Power-Harnessing the Potential Energy of Water for Small-Scale Electricity Generation', *IJRASHT*, pp. 13–17, Sep. 2024, doi: 10.71143/4p12n447.
[37] V. LABORIE and S. LADREYT, 'Information on spillways-Summary of flow laws at weirs and spillways', CETMEF, France, Hydraulics at the level of structures, Feb. 2025.
[38] A. A. Ali, D. Alfarge, A. M. Lafta, M. I. Hasan, and F. L. Rashid, 'Numerical investigation for the effects of surface roughness in counter flow microchannel heat exchanger with different channels geometries', *Discov Appl Sci*, vol. 6, no. 9, p. 459, Aug. 2024, doi: 10.1007/s42452-024-06132-5.
[39] D. R. Ray and D. K. Das, 'Simulations of Flows via CFD in Microchannels for Characterizing Entrance Region and Developing New Correlations for Hydrodynamic Entrance Length', *Micromachines*, vol. 14, no. 7, p. 1418, Jul. 2023, doi: 10.3390/mi14071418.
[40] K. Glock, M. Tritthart, H. Habersack, and C. Hauer, 'Comparison of Hydrodynamics Simulated by 1D, 2D and 3D Models Focusing on Bed Shear Stresses', *Water*, vol. 11, no. 2, p. 226, Jan. 2019, doi: 10.3390/w11020226.
[41] H. Canilho and C. Fael, 'Velocity Field Analysis of a Channel Narrowed by Spur-dikes to Maximize Power Output of In-stream Turbines', *J. sustain. dev. energy water environ. syst.*, vol. 6, no. 3, pp. 534–546, Sep. 2018, doi: 10.13044/j.sdewes.d6.0197.
[42] C. B. Amougou, D. Tsuanyo, D. Fioriti, J. Kenfack, A. Aziz, and P. Elé Abiama, 'LCOE-Based Optimization for the Design of Small Run-of-River Hydropower Plants', *Energies*, vol. 15, no. 20, p. 7507, Oct. 2022, doi: 10.3390/en15207507.
[43] M. Rumbayan and R. Rumbayan, 'Feasibility Study of a Micro Hydro Power Plant for Rural Electrification in Lalumpe Village, North Sulawesi, Indonesia', *Sustainability*, vol. 15, no. 19, p. 14285, Sep. 2023, doi: 10.3390/su151914285.
[44] S. BELLAHCEN, 'Numerical and experimental study of the velocity field in compound channels', University of Strasbourg, Strasbourg, France, 2016.